JOURNAL OF Materials CHEMISTRY
Feature Article

Defect chemistry of the BIMEVOXes†

Isaac Abrahams*[a] and Franciszek Krok[b]

[a]*Structural Chemistry Group, Department of Chemistry, Queen Mary, University of London, Mile End Road, London, UK E1 4NS*
[b]*Faculty of Physics, Warsaw University of Technology, ul. Koszykowa 75, 00-662 Warsaw, Poland*

Received 24th April 2002, Accepted 18th July 2002
First published as an Advance Article on the web 27th September 2002

Since their discovery in 1988, the BIMEVOXes have been the subject of significant research due to their high oxide ion conductivity at relatively low temperatures. The development of these materials is briefly reviewed. The defect structure of the BIMEVOXes is discussed and used to construct general defect equations for solid solution formation. Two limiting models are proposed by which solid solution formation can occur. In the *Equatorial Vacancy* (EV) model, vacancies are located exclusively in bridging sites in the vanadate layer. In contrast, the *Apical Vacancy* (AV) model assumes vacancies are located exclusively in non-bridging apical sites in the vanadate layer. The general defect equations can be used to predict theoretical solid solution limits for all types of substitutions for vanadium in $Bi_4V_2O_{11-\delta}$. These limits are found to vary not only with the charge of the dopant ion, but also with the coordination number of the metal dopant. In most cases it is found that the EV model yields theoretical solid solution limits close to those observed. The EV model is also used to present a mechanism for ionic conduction in BIMEVOXes, which involves movement of equatorial oxide ions/vacancies between vanadium octahedra and tetrahedra with the formation of a five-coordinate vanadium intermediate.

1 Introduction

Solids that show high conductivity in the absence of a significant electronic contribution are generally known as superionic conductors or solid electrolytes. Their ionic conductivities are in many cases comparable to those of the best liquid electrolytes. Unlike their liquid counterparts, solid electrolytes show conduction of either anions or cations, but generally not both. While much research has focussed on materials which show fast conduction of cations, such as Ag^+, Na^+ and Li^+, a significant amount of work has also gone into the development of anion conducting solids, particularly O^{2-} ion conductors. The main interest in oxide ion conducting systems stems from their application as electrolytes in fuel cells, oxygen pumps and gas sensors.[1] This work has predominantly involved studies on fluorite related systems, in particular the stabilised zirconias, which show high conductivities in the order of 10^{-1} S cm^{-1} at temperatures around 1000 °C.[1] Bi_2O_3 exhibits a stable fluorite phase (δ) at temperatures above 730 °C,[2] and much work has been carried out on stabilisation of this phase to lower temperatures through solid solution formation.[3–7]

In 1988 Abraham *et al.*[8] published their first paper on $Bi_4V_2O_{11}$. This compound showed remarkably high conductivity in the order of 10^{-2} S cm^{-1} at temperatures around 600 °C. It was this feature of the new material, which appeared to offer significant improvements over the stabilised zirconias. This group also described a new class of O^{2-} ion conductors based on cation substitution for vanadium in $Bi_4V_2O_{11}$.[9] These materials were dubbed the BIMEVOXes (BI = bismuth, ME = metal dopant, V = vanadium, OX = oxide) and became the focus of a great deal of attention over the following years due to their extremely high conductivities at relatively low temperatures; in the order of 10^{-3} S cm^{-1} at 300 °C.

The aim of this article is to bring together some of the work on the BIMEVOXes and the parent compound, $Bi_4V_2O_{11-\delta}$, and show how by combining the knowledge gained from these studies an understanding of the defect chemistry and conductivity mechanism emerges.

2 Synthetic considerations

$Bi_4V_2O_{11-\delta}$ is the end member of a solid solution that occurs in the Bi_2O_3–V_2O_5 system between 66.7 to 70.4% Bi_2O_3.[10] In practice it is difficult to prepare stoichiometric $Bi_4V_2O_{11-\delta}$ free from $BiVO_4$ and often excess Bi_2O_3 is used in order to obtain phase pure materials. Synthesis conditions are critical in determining the oxygen stoichiometry,[11,12] with vanadium exhibiting both +4 and +5 oxidation states in this system. The degree of reduction is reflected in the value of δ. Samples prepared in air at 850 °C and quenched to room temperature show significant vanadium reduction, are dark brown in colour, have strong EPR signals and exhibit weak paramagnetism.[12] In contrast, samples that are slow cooled in oxygen are deep red in colour and show negligible EPR signals and magnetic susceptibilities. Under suitable reducing conditions the pure V^{IV} system, $Bi_4V_2O_{10}$ can be obtained, which shows V in a five coordinate environment.[13] It should be noted that a form of this compound has also been synthesised with the fluorite structure.[14] The variations in δ are also observed in the BIMEVOXes,‡ for example in BIMGVOX, $Bi_2Mg_xV_{1-x}O_{5.5-3x/2-\delta}$, refinement of oxygen occupancies using high resolution neutron diffraction data reveal a significant difference in the value of δ between slow cooled and quenched samples (0.040 and 0.076 respectively).[15] Recently some V^{IV} analogues of BIMEVOX systems have been synthesised such

†Electronic supplementary information (ESI) available: full list of schemes for all combinations of *l* and *CN* generated using the program DEFEQN. A listing of the program is also available. See http://www.rsc.org/suppdata/jm/b2/b203992n/

‡The value of δ in the conventional formulae of BIMEVOX solid solutions corresponds to half that in the parent compound, $Bi_4V_2O_{11-\delta}$.

as $Bi_2Sb_xV_{1-x}O_{5+x/2}$,[16] $Bi_2Ge_xV_{1-x}O_5$, $Bi_2Ti_xV_{1-x}O_5$ and $Bi_2Fe_xV_{1-x}O_{5-x/2}$.[17]

Unlike $Bi_4V_2O_{11-\delta}$, phase-pure (by X-ray and neutron diffraction) BIMEVOXes are readily prepared from stoichiometric ratios of the parent oxides. Generally polycrystalline BIMEVOXes have been synthesised by standard solid state reaction of their parent oxide powders at high temperatures. However, low temperature routes such as co-precipitation followed by low temperature firing[18] and mechanochemical activation[14,19,20] have been successfully employed in the synthesis of fine-grained $Bi_4V_2O_{11-\delta}$. BIMEVOX thin films have been obtained using sol–gel routes,[21] chemical vapour deposition[22] and laser deposition,[23] while single crystals can be grown from the melt.[24,25] Densification of materials, which results in minimisation of grain boundary resistances, is usually carried out through high temperature sintering. However, recent studies show the potential of other methods of densification such as melting[26] and the addition of a sintering agent like zirconia.[27] Synthesis times of many hours using conventional methods have been reduced to a few minutes using microwave radiation.[28]

3 Basic structural aspects

3.1 $Bi_4V_2O_{11-\delta}$

In order to describe the structures adopted by the BIMEVOXes it is helpful to start with that of the parent material, $Bi_4V_2O_{11-\delta}$. The parent compound shows complex polymorphism, with three principal phases, α, β and γ, having been identified. The room temperature stable phase, α-$Bi_4V_2O_{11-\delta}$, crystallises with monoclinic symmetry,[29,30] however low levels of impurities in the starting materials stabilise an orthorhombic form with cell dimensions $a = 16.6$, $b = 16.8$, $c = 15.4$ Å.[2] On heating, phase transitions to β- (447 °C) and γ- (567 °C) polymorphs are observed in the differential thermal analysis (DTA) trace of $Bi_4V_2O_{11-\delta}$, with corresponding changes in the Arrhenius plot of conductivity.[8] The existence of two other phases, one just before melting on heating, and a second, α′, on cooling have been reported,[8] however these phases have never been fully characterised.

The phase transitions are associated with vacancy ordering in the oxide sublattice and the crystallographic relationships of the various polymorphs have been characterised with respect to a mean orthorhombic cell[2,29,31] of dimensions $a_m \approx 5.53$, $b_m \approx 5.61$, $c_m \approx 15.28$ Å, *viz*: α-orthorhombic, $a \approx 3a_m$, $b \approx b_m$, $c \approx c_m$; α-monoclinic, $a \approx 6a_m$, $b \approx b_m$, $c \approx c_m$, $\beta = 89.756°$; β (orthorhombic), $a \approx 2a_m$, $b \approx b_m$, $c \approx c_m$; γ (tetragonal), $a \approx a_m/\sqrt{2}$, $c \approx c_m$. Of interest to most researchers is the fully disordered tetragonal γ-phase, which shows exceptionally high conductivity at relatively low temperatures.

An idealised structural model of γ-$Bi_4V_2O_{11-\delta}$ can be obtained by considering it to be derived from the structure of γ-Bi_2MoO_6.[32] The structure of γ-$Bi_4V_2O_{11-\delta}$ (Fig. 1) consists of alternating layers of $[Bi_2O_2]_n^{n2+}$ and $[VO_{3.5-\delta}\ \square_{0.5+\delta}]_n^{n2-}$ (where □ represents an oxide ion vacancy). The $[Bi_2O_2]_n^{n2+}$ layers exhibit Bi in a square pyramidal coordination with four Bi–O bonds of approximate length 2.3 Å. The Bi $6s^2$ lone pairs are stereochemically active and point to vacant sites between four corner sharing vanadium polyhedra in the vanadate layers. The bismuthate layers sandwich the vanadate layers with lone pair orbitals pointing directly towards each other through the vacant site in the vanadate layer. This interstitial site is therefore linearly "coordinated" to two Bi $6s^2$ lone pair orbitals. The inter-layer interaction is essentially ionic in nature, but it should be noted that in α-$Bi_4V_2O_{11-\delta}$ there is a greater degree of covalency evident in the inter-layer contacts than is seen in the BIMEVOXes.[29]

In the idealised structure, vanadium is in a regular octahedral environment with oxygen. Vanadium octahedra share corners to give the two dimensional network. However, the incorporation of significant numbers of vacancies in the vanadate layer requires lower coordination numbers for some of the vanadium polyhedra. In the crystal structure of α-$Bi_4V_2O_{11-\delta}$, significant deviations from the idealised structure are observed.[29] In fact recent studies suggest the likelihood of both four- and five-coordinate vanadium polyhedra.[30] Distortions within the vanadium polyhedra lead to ferroelectric behaviour with maximum permitivity at the α↔β phase transition.[10,33]

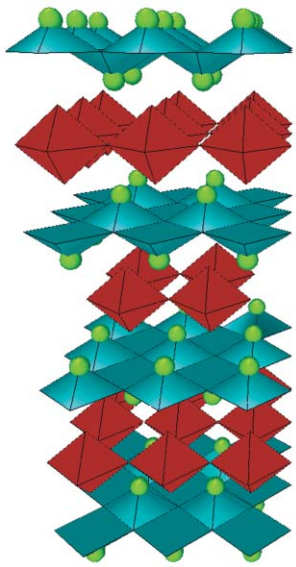

Fig. 1 Idealised structure of γ-$Bi_4V_2O_{11-\delta}$. Red octahedra represent VO_6, Bi atoms are illustrated by spheres. Equatorial vacancies have been omitted for clarity.

3.2 The BIMEVOXes

$Bi_4V_2O_{11-\delta}$ is an unusual compound in that it forms substitutional solid solutions with most binary metal oxides almost irrespective of the radius of the substituting metal ion.[9,32] By far the most studied BIMEVOXes are the divalent substituted systems with general formula $Bi_2M^{II}{}_xV_{1-x}O_{5.5-3x/2-\delta}$. At low values of x (*x ca.* < 0.10) the orthorhombic α or β phases are stabilised at room temperature. γ-Phase stabilisation generally occurs between $x \approx 0.10$ to 0.13 for the divalent substituted systems, although there is some discrepancy between studies from different groups. Interestingly, the "tetragonal" γ-phase seen in these systems shows weak neutron diffraction peaks that are attributed to an incommensurate superlattice.[34–37] This incommensurate modulated phase has been termed γ′. On heating, the γ′-superlattice peaks disappear and the only peaks of the commensurate γ-phase are seen in neutron diffraction patterns (Fig. 2).[35,36] The γ′–γ (order–disorder) transition can be correlated with a change in the Arrhenius plot of conductivity (Fig. 3) at around 500 °C.[35] Samples quenched from high temperatures show the regular γ-phase structure with an absence of superlattice reflections and have enabled detailed studies of the defect structure of the γ-phase to be carried out at ambient temperatures.[15,38,39] We believe that the modulation arises due to small changes in oxygen stoichiometry, through V oxidation/reduction. It is interesting to note that time dependent isothermal measurements of ionic conductivity in BIZNVOX have shown a lowering of conductivity with time and seem to support this view.[40]

Initial studies on tetragonal-BICUVOX indicated significant disorder in the vanadate layer,[9] similar to that in the γ-polymorph of the parent material, $Bi_4V_2O_{11-\delta}$. However, at that time the nature of the disorder was not well resolved. Subsequent studies on BICOVOX, using neutron diffraction, confirmed

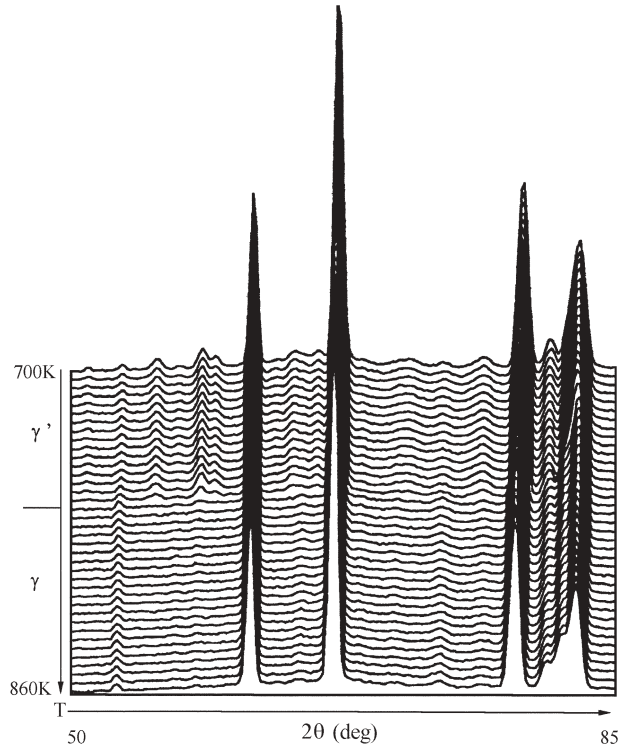

Fig. 2 Neutron powder diffraction patterns for BICOVOX.15, $Bi_2Co_{0.15}V_{0.90}O_{5.275-\delta}$, showing the γ' to γ phase transition on heating. Reprinted from ref. 36 with permission from Elsevier Science B.V.

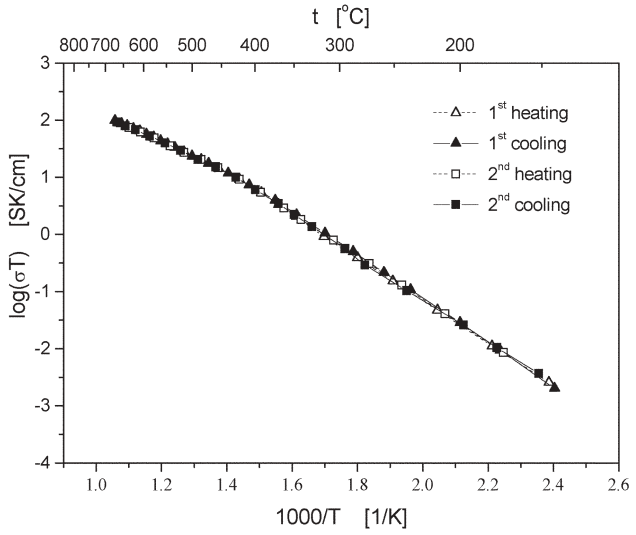

Fig. 3 Arrhenius plot of total conductivity for BINIVOX.14, $Bi_2Ni_{0.14}V_{0.86}O_{5.29-\delta}$, showing γ'-phase (low temperature) and γ-phase (high temperature) regions.

significant disorder in both apical and equatorial oxygens in the vanadate layer.[37] Fourier maps generated from powder neutron diffraction data for BIMEVOXes show delocalised scattering around the vanadate layer oxygen atoms (Fig. 4).

Over a number of years we have carried out detailed investigations of the defect structures of a range of divalent substituted γ-BIMEVOXes (BICOVOX,[38] BINIVOX[39] and BIMGVOX[15]) using high-resolution powder neutron diffraction. Studies on the quenched γ-BIMEVOXes have confirmed that there is significant disorder in the oxide sites in the vanadate layer and that the high temperature tetragonal γ-phase structure is preserved by rapid quenching. The disorder is limited to the vanadate layer oxygens, while vacancies appear

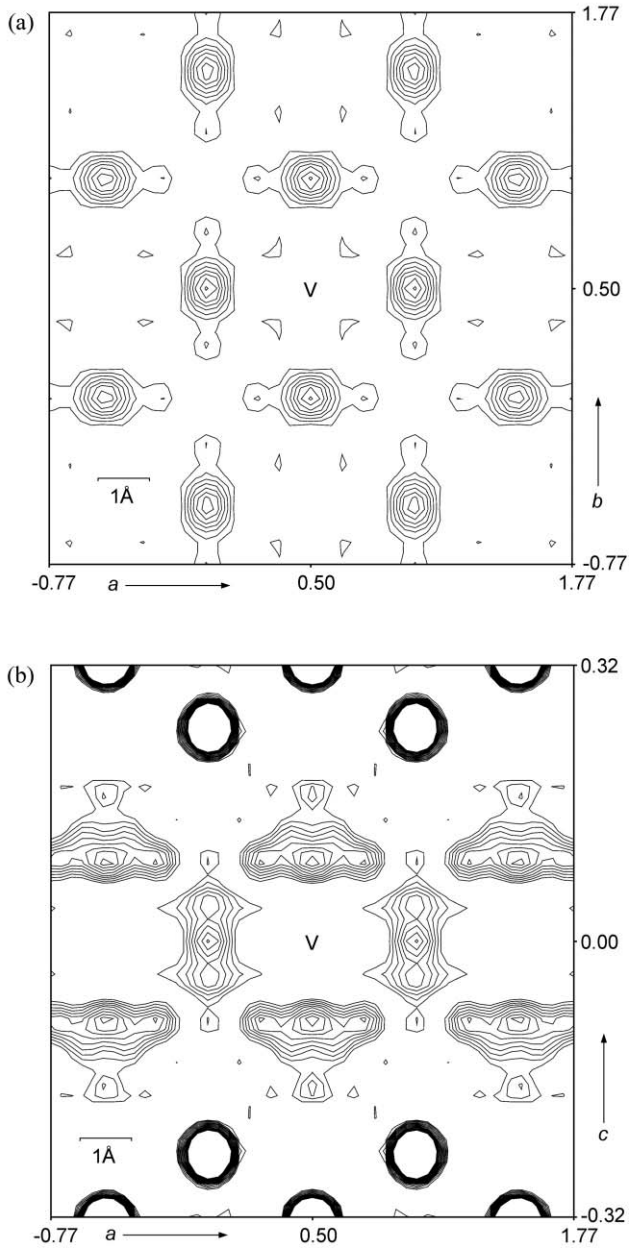

Fig. 4 Fourier maps generated from powder neutron diffraction data for quenched γ-BIMGVOX.10, $Bi_2Mg_{0.10}V_{0.90}O_{5.35-\delta}$, showing diffuse scattering from oxide positions in the vanadate layer. (a) Section of a–b plane at $z = 0$, (b) section of a–c plane at $y = 0.5$.

to be concentrated in the equatorial planes of these layers. Table 1 shows the refined structural parameters for γ-$Bi_2Mg_{0.1}V_{0.9}O_{5.35-\delta}$, which are typical.[15] Three vanadate layer oxide sites have been identified (Fig. 5a). O(2) and O(4) are nominally apical oxygens and are coordinated to one V/M atom only (where M is the dopant metal). The ratio of the summed occupancy of O(2) and O(4) per V/M atom is 2 : 1 and thus the nominal apical (non-bridging) position is full. O(3) is nominally an equatorial (bridging) position and may be coordinated to two V/M atoms. The vacancies are concentrated on the O(3) site.

Consideration of the refined site occupancies and the inter-site contact distances allows the defect structure to be determined. From this two principal types of polyhedra emerge *viz*: distorted octahedra (Fig. 5b) and distorted tetrahedra (Fig. 5c). O(2) is exclusively associated with the octahedra, O(4) is exclusive to the tetrahedra and O(3) is common to both coordinations. The presence of predominantly two types of V environment has also been confirmed

Table 1 Refined structural parameters for γ-BIMGVOX.10,[a 15] $Bi_2V_{0.9}Mg_{0.1}O_{5.35-\delta}$

Atom	Site	x	y	z	Occupancy	U_{iso}/Å^2
Bi	4e	0.0(—)	0.0(—)	0.16917(7)	1.0(—)	0.0385(5)
V/Mg	2b	0.5(—)	0.5(—)	0.0(—)	0.9/0.1(—)	0.025(—)
O(1)	4d	0.0(—)	0.5(—)	0.25(—)	1.0(—)	0.0342(6)
O(2)	4e	0.5(—)	0.5(—)	0.1097(8)	0.279(10)	0.057(2)
O(3)	8g	0.5(—)	0.0(—)	0.0295(3)	0.319(8)	0.087(2)
O(4)	16n	0.5(—)	0.3160(24)	0.0920(4)	0.180(3)	0.057(2)

[a] a = 3.93535(5), c = 15.4489(2) Å, space group *I*4/*mmm*.

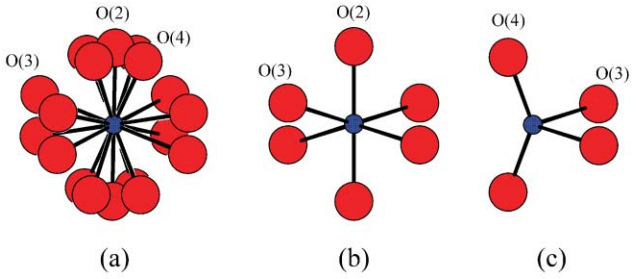

Fig. 5 Refined oxygen positions in BIMGVOX.10, $Bi_2Mg_{0.10}V_{0.90}O_{5.35-\delta}$, corresponding to data in Table 1. (a) Average situation, (b) distorted octahedron, (c) distorted tetrahedron.

by ^{51}V solid state NMR in the parent orthorhombic α-$Bi_4V_2O_{11-\delta}$.[12] These results also indicate the presence of small amounts of five-coordinate V in samples prepared under certain cooling conditions. The exclusivity of O(2) and O(4) to octahedra and tetrahedra respectively allows the relative fractions of these vanadium polyhedra to be easily calculated from the neutron refinements as follows.

Let $F_{O(m)}$ be the fractional occupancy per V/M atom of a particular oxygen site m. The structure refinements indicate that the total apical (non-bridging) oxygen per metal atom is always 2 (eqn. (1)).

$$F_{O(2)} + F_{O(4)} = 2 \quad (1)$$

Since the equatorial (bridging) oxygen O(3) is associated with both tetrahedra and octahedra, the total O(3) occupancy will have two basic components (eqn. (2)).

$$F_{O(3)} = F_{O(3oct)} + F_{O(3tet)} \quad (2)$$

The apical oxygen O(2) is associated exclusively with octahedra. Therefore:

$$F_{O(3oct)} = F_{O(2)} \quad (3)$$

Similarly the apical oxygen O(4) is associated exclusively with tetrahedra and taking into account relative site multiplicities:

$$F_{O(3tet)} = F_{O(4)}/2 \quad (4)$$

Therefore the fractions, X, of octahedra and tetrahedra are given by:

$$X_{oct} = F_{O(2)}/2 = F_{O(3oct)}/2 \quad (5)$$

$$X_{tet} = F_{O(4)}/2 = F_{O(3tet)} \quad (6)$$

Hence as x increases the number of vacancies increase and consequently X_{tet} also increases.

In a BIMEVOX system where V is substituted by metal M of charge l+, then assuming that Bi is only present in the trivalent state (which is evident by the coordination adopted), the overall charge on the $[V_{1-x}M^{l+}{}_xO_{3.5-(5-l)x/2-\delta}]_n$ layer must be $2n-$ to preserve electroneutrality. Taking this into account, and subtracting the contribution to the layer charge from M^{l+} (lx), the effective valence charge on vanadium, Z_{eff}, may be calculated as follows:

$$Z_{eff} = \frac{2(F_{O(2)} + F_{O(3)} + F_{O(4)}) - (2 + lx)}{1 - x} \quad (7)$$

The value of δ may also readily be calculated as follows:

$$\delta = 3.5 - (5 - l)x/2 - (F_{O(2)} + F_{O(3)} + F_{O(4)}) \quad (8)$$

In these calculations it is assumed that substitution is exclusive to the V site and that there is no incorporation of excess Bi into the vanadate layer. It is therefore possible to extract quite detailed information on the local defect structure from a structure averaging technique such as neutron diffraction.

4 Defect chemistry of the BIMEVOXes

In order to describe the defect chemistry of the BIMEVOXes it is helpful to introduce a symbolism based on the Kröger–Vink notation.[41] A key to the notation used is given in Table 2. Note, that the symbols *a* and *e* are used to represent apical (non-bridging) and equatorial (bridging) positions respectively

Table 2 Key to defect notation in BIMEVOX systems

Symbol	Description
V_V	Vanadium located in its normal lattice site
$M_V^{(5-l)\prime}$	Dopant metal atom located on a vanadium site with effective charge $-(5-l)$, where l is the charge on the metal ion M^{l+}
O_{Oe}	Neutral equatorial oxygen in its normal lattice site
O_{Oe}''	Equatorial oxygen with effective charge −2
O_{Oe}'	Equatorial oxygen with effective charge −1
$O_{Oe,(CN-4)/2}^{(CN-5)\prime}$	$(CN-4)/2$ equatorial oxygens each with effective charge $-(CN-5)$
O_{Oa}	Neutral apical oxygen in its normal lattice site
O_{Oa}''	Apical oxygen with effective charge −2
O_{Oa}'	Apical oxygen with effective charge −1
$O_{Oa,CN-4}''$	$CN-4$ apical oxygens each with effective charge −2
$\square_{Oe}$	Neutral equatorial oxygen vacancy
$\square_{Oe}^{\cdot\cdot}$	Equatorial oxygen vacancy with effective charge of +2
$\square_{Oe}^{\cdot}$	Equatorial oxygen vacancy with effective charge of +1
$\square_{Oa}$	Neutral apical oxygen vacancy
$\square_{Oa}^{\cdot\cdot}$	Apical oxygen vacancy with effective charge of +2
$\square_{Oa}^{\cdot}$	Apical oxygen vacancy with effective charge of +1
$O_{is,(CN-6)/2}''$	$(CN-6)/2$ bridging interstitial oxygens each with effective charge −2
$O_{iu,CN-6}''$	$CN-6$ non-bridging interstitial oxygens each with effective charge −2

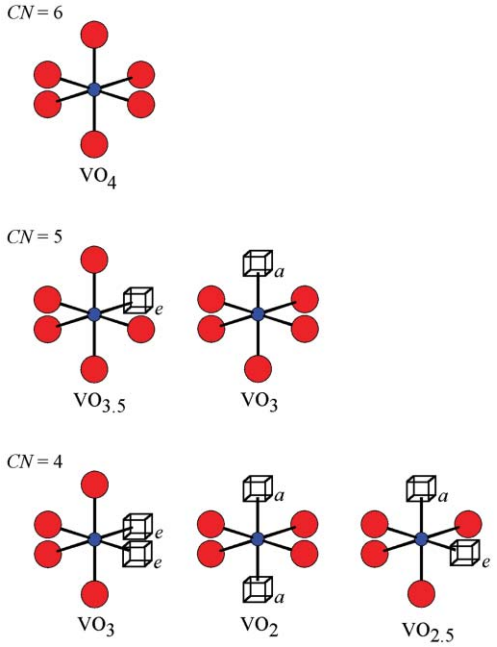

Fig. 6 Schematic representation of possible vanadium coordination environments in BIMEVOXes involving equatorial and/or apical vacancies.

and that the symbol □ is used to represent a vacancy in preference to *V* to avoid confusion with vanadium. Starting from the idealised structure shown in Fig. 1, there are two basic locations for an oxide vacancy in the vanadate layer. Vacancies can either be located on the non-bridging apical positions, $\square_{Oa}$, or the bridging equatorial positions, $\square_{Oe}$. Vanadium is known to adopt coordination numbers of four, five and six in oxide systems[42] and there are a number of possible ways in which vanadium can achieve these coordinations in BIMEVOXes (Fig. 6). The general formula of the vanadate layer in a BIMEVOX assuming only substitution of vanadium by M^{l+} is given by $[V_{1-x}M^{l+}{}_xO_{3.5-(5-l)3x/2-\delta}\square_{0.5+(5-l)3x/2+\delta}]_n^{2n-}$. Assuming that dopant ions show a preference for a particular coordination number with oxygen (four to eight), it is possible to describe the defect chemistry of the BIMEVOXes by considering two limiting models. The *Equatorial Vacancy* (EV) model assumes that all vacancies are located on the equatorial (bridging) oxygen sites. Similarly the *Apical Vacancy* (AV) model assumes that all vacancies are located in the apical (non-bridging) oxygen sites. Assuming the presence of only octahedra and tetrahedra, the two models predict different fractions of octahedra and tetrahedra (X_{oct} and X_{tet} respectively) at particular vacancy concentrations (Fig. 7). In the parent compound $Bi_4V_2O_{11-\delta}$, which has an intrinsic vacancy concentration of 0.5 per V atom (assuming δ to be negligible), the AV model predicts a 3 : 1 ratio of octahedra to tetrahedra, while in the EV model this ratio is 1 : 1. It should be noted that from the diffraction results there is no way of distinguishing between five-coordinate vanadium polyhedra and a 1 : 1 average of vanadium octahedra and tetrahedra. Therefore in the parent compound, the EV model predicts that the average vanadium polyhedron is five-coordinate and may be described by $V_VO_{Oa,2}O_{Oe,1.5}\square_{Oe,0.5}$, while in the AV model the average vanadium polyhedron has 75% octahedral and 25% tetrahedral character and is described by $V_VO_{Oa,1.5}\square_{Oa,0.5}O_{Oe,2}$, *i.e.* an average coordination number of 5.5.

In order to understand the influences of aliovalency and coordination number (*CN*) of the dopant on the defect chemistry of the BIMEVOXes it is helpful to look at the example of the divalent substituted systems. When a divalent metal is introduced to a V site an effective charge of −3 on the

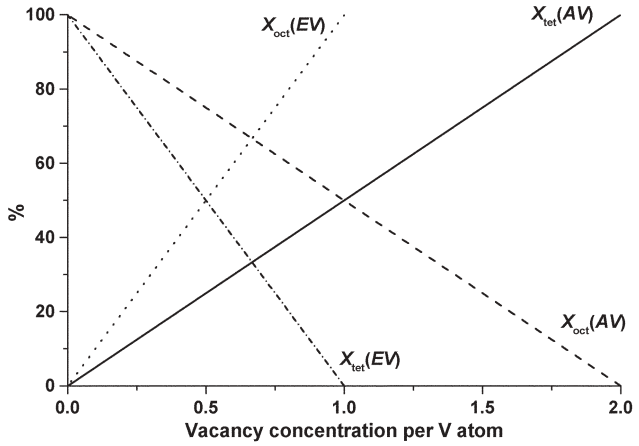

Fig. 7 Variations of X_{oct} and X_{tet} with vacancy concentration in EV and AV models.

site results. Electroneutrality is maintained by the creation of 1.5 vacancies in the oxide sublattice. Depending on the *CN* of the dopant metal and the vacancy model used, all, some or none of these vacancies will be trapped on the metal dopant polyhedron. The various substitution schemes are summarised in Table 3. In the EV model, when the divalent metal dopant has a preferred *CN* of four, electroneutrality dictates that substitution of two vanadium atoms in octahedral sites is accompanied by the conversion of a vanadium octahedron to a tetrahedron (Scheme 1a), while substitution of two vanadium atoms in tetrahedral sites requires the conversion of three vanadium octahedra to tetrahedra (Scheme 1b). Substitution of vanadium in an average vanadium polyhedron gives an overall effective charge of −2 on the resulting dopant metal tetrahedron and consequently must be accompanied by conversion of two further average vanadium polyhedra to tetrahedra. Therefore on average only one in three vanadium atoms can be substituted (Scheme 1c).

In the AV model, substitution of four vanadium atoms in octahedral sites is accompanied by the conversion of one vanadium tetrahedron to an octahedron *i.e.* the formation of oxide interstitials (Scheme 2a). In contrast, substitution of four vanadium atoms in tetrahedral sites yields additional vacancies in the form of three vanadium tetrahedra (Scheme 2b). Since in the parent compound there are 75% octahedra, the average situation is dominated by Scheme 2a resulting in no additional vanadium octahedra or tetrahedra being formed (Scheme 2c).

Similar substitution schemes can be written for all possible

Table 3 Reaction schemes for substitution of V in BIMEVOXes by M^{2+} ions with preferred coordination number, $CN = 4$

Scheme 1 EV model.
(a) Substitution for octahedral vanadium
$(V_VO_{Oa,2}O_{Oe,2}) + 0.5(V_VO_{Oa,2}O_{Oe,2}) \rightarrow (M_V'''O_{Oa,2}O_{Oe}\square_{Oe}^{\bullet\bullet}) + 0.5(V_VO_{Oa,2}O_{Oe}\square_{Oe}^{\bullet\bullet})$
(b) Substitution for tetrahedral vanadium
$(V_VO_{Oa,2}O_{Oe}\square_{Oe}) + 1.5(V_VO_{Oa,2}O_{Oe,2}) \rightarrow (M_V'''O_{Oa,2}O_{Oe}\square_{Oe}) + 1.5(V_VO_{Oa,2}O_{Oe}\square_{Oe}^{\bullet\bullet})$
(c) Substitution for average vanadium polyhedron
$3(V_VO_{Oa,2}O_{Oe,1.5}\square_{Oe,0.5}) \rightarrow (M_V'''O_{Oa,2}O_{Oe}\square_{Oe}^{\bullet}) + 2(V_VO_{Oa,2}O_{Oe}\square_{Oe}^{\bullet})$

Scheme 2 AV model.
(a) Substitution for octahedral vanadium
$(V_VO_{Oa,2}O_{Oe,2}) + 0.25(V_V\square_{Oa,2}O_{Oe,2}) \rightarrow (M_V'''\square_{Oa,2}^{\bullet\bullet}O_{Oe,2}) + 0.25(V_VO_{Oa,2}''O_{Oe,2})$
(b) Substitution for tetrahedral vanadium
$(V_V\square_{Oa,2}O_{Oe,2}) + 0.75(V_VO_{Oa,2}O_{Oe,2}) \rightarrow (M_V'''\square_{Oa,2}O_{Oe,2}) + 0.75(V_V\square_{Oa,2}^{\bullet\bullet}O_{Oe,2})$
(c) Substitution for average vanadium polyhedron
$(V_VO_{Oa,1.5}\square_{Oa,0.5}O_{Oe,2}) \rightarrow (M_V'''\square_{Oa,2}^{1.5\bullet}O_{Oe,2})$

Table 4 General schemes for substitution of V in BIMEVOXes by M^{l+} ions with preferred coordination number *CN* (where $4 \leqslant CN \leqslant 6$)

Scheme 3 EV model, $4 \leqslant CN \leqslant 6$, vacancies created.
(a) Substitution for vanadium octahedron, where $CN > (l + 1)$.
$\frac{CN+1-l}{2}(V_VO_{Oa,2}O_{Oe,2}) \rightarrow (M_V^{(5-l)\prime}O_{Oa,2}O_{Oe,1+(CN-4)/2}\square_{Oe,(6-CN)/2}^{\cdot\cdot}) + \frac{CN-1-l}{2}(V_VO_{Oa,2}O_{Oe}\square_{Oe}^{\cdot\cdot})$
(b) Substitution for vanadium tetrahedron, where $CN > (l - 1)$.
$(V_VO_{Oa,2}O_{Oe}\square_{Oe}) + \frac{CN+1-l}{2}(V_VO_{Oa,2}O_{Oe,2}) \rightarrow (M_V^{(5-l)\prime}O_{Oa,2}O_{Oe}O_{Oe,(CN-4)/2}{}''\square_{Oe,(6-CN)/2}) + \frac{CN+1-l}{2}(V_VO_{Oa,2}O_{Oe}\square_{Oe}^{\cdot})$
(c) Substitution for average vanadium polyhedron, where $CN > l$.
$(CN + 1 - l)(V_VO_{Oa,2}O_{Oe,1.5}\square_{Oe,0.5}) \rightarrow (M_V{}^{(5-l)\prime}O_{Oa,2}O_{Oe}O_{Oe,(CN-4)/2}{}^{(CN-5)\prime}\square_{Oe,(6-CN)/2}{}^{(5-CN)\cdot}) + (CN - l)(V_VO_{Oa,2}O_{Oe}\square_{Oe}^{\bullet})$

Scheme 4 EV model, $4 \leqslant CN \leqslant 6$, vacancies consumed.
(a) Substitution for vanadium octahedron, where $CN < (l + 1)$.
$(V_VO_{Oa,2}O_{Oe,2}) + \frac{l+1-CN}{2}(V_VO_{Oa,2}O_{Oe}\square_{Oe}) \rightarrow (M_V^{(5-l)\prime}O_{Oa,2}O_{Oe,1+(CN-4)/2}\square_{Oe,(6-CN)/2}^{\cdot}) + \frac{l+1-CN}{2}(V_VO_{Oa,2}O_{Oe}O_{Oe}'')$
(b) Substitution for vanadium tetrahedron, where $CN < (l - 1)$.
$\frac{l+1-CN}{2}(V_VO_{Oa,2}O_{Oe}\square_{Oe}) \rightarrow (M_V^{(5-l)\prime}O_{Oa,2}O_{Oe}O_{Oe,(CN-4)/2}{}''\square_{Oe,(6-CN)/2}) + \frac{l-1-CN}{2} + (V_VO_{Oa,2}O_{Oe}\square_{Oe}'')$
(c) Substitution for average vanadium polyhedron, where $CN < l$.
$(l - CN + 1)(V_VO_{Oa,2}O_{Oe,1.5}\square_{Oe,0.5}) \rightarrow (M_V{}^{(5-l)\prime}O_{Oa,2}O_{Oe}O_{Oe,(CN-4)/2}{}^{(CN-5)\prime}\square_{Oe,(6-CN)/2}{}^{(5-CN)\bullet}) + (l - CN)(V_VO_{Oa,2}O_{Oe}O_{Oe}')$

Scheme 5 EV model, $4 \leqslant CN \leqslant 6$, no net change in vacancies.
(a) Substitution for vanadium octahedron, where $CN = (l + 1)$.
$(V_VO_{Oa,2}O_{Oe,2}) \rightarrow (M_V{}^{(5-l)\prime}O_{Oa,2}O_{Oe,1+(CN-4)/2}\square_{Oe,(6-CN)/2}^{\bullet\bullet})$
(b) Substitution for vanadium tetrahedron, where $CN = (l - 1)$.
$(V_VO_{Oa,2}O_{Oe}\square_{Oe}) \rightarrow (M_V{}^{(5-l)\prime}O_{Oa,2}O_{Oe}O_{Oe,(CN-4)/2}{}''\square_{Oe,(6-CN)/2})$
(c) Substitution for average vanadium polyhedron, where $CN = l$.
$(V_VO_{Oa,2}O_{Oe,1.5}\square_{Oe,0.5}) \rightarrow (M_V{}^{(5-l)\prime}O_{Oa,2}O_{Oe}O_{Oe,(CN-4)/2}{}^{(CN-5)\prime}\square_{Oe,(6-CN)/2}{}^{(5-CN)\bullet})$

Scheme 6 AV model, $4 \leqslant CN \leqslant 6$, vacancies created.
(a) Substitution for octahedral vanadium, where $2CN > (l + 7)$
$\frac{2CN-3-l}{4}(V_VO_{Oa,2}O_{Oe,2}) \rightarrow (M_V^{(5-l)\prime}O_{Oa,CN-4}\square_{Oa,6-CN}^{\cdot\cdot}O_{Oe,2}) + \frac{2CN-7-l}{4}(V_V\square_{Oa,2}{}^{\cdot\cdot}O_{Oe,2})$
(b) Substitution for tetrahedral vanadium, where $2CN > (l + 3)$
$(V_V\square_{Oa,2}O_{Oe,2}) + \frac{2CN-3-l}{4}(V_VO_{Oa,2}O_{Oe,2}) \rightarrow (M_V^{(5-l)\prime}O_{Oa,CN-4}{}''\square_{Oa,6-CN}O_{Oe,2}) + \frac{2CN-3-l}{4}(V_V\square_{Oa,2}{}^{\cdot\cdot}O_{Oe,2})$
(c) Substitution for average vanadium polyhedron, where $2CN > (l + 6)$.
$\frac{2CN-3-l}{3}(V_VO_{Oa,1.5}\square_{Oa,0.5}O_{Oe,2}) \rightarrow (M_V^{(5-l)\prime}O_{Oa,CN-4}{}^{(5.5-CN)(5-CN)\prime}\square_{Oa,6-CN}{}^{(5.5-CN)(CN-3)\cdot}O_{Oe,2}) + \frac{2CN-6-l}{3}(V_V\square_{Oa,2}{}^{1.5\cdot}O_{Oe,2})$

Scheme 7 AV model, $4 \leqslant CN \leqslant 6$, vacancies consumed.
(a) Substitution for octahedral vanadium, where $2CN < (l + 7)$
$(V_VO_{Oa,2}O_{Oe,2}) + \frac{l+7-2CN}{4}(V_V\square_{Oa,2}O_{Oe,2}) \rightarrow (M_V{}^{(5-l)\prime}O_{Oa,CN-4}\square_{Oa,6-CN}{}^{\cdot\cdot}O_{Oe,2}) + \frac{l+7-2CN}{4}(V_VO_{Oa,2}{}''O_{Oe,2})$
(b) Substitution for tetrahedral vanadium, where $2CN < (l + 3)$
$\frac{l+7-2CN}{4}(V_V\square_{Oa,2}O_{Oe,2}) \rightarrow (M_V{}^{(5-l)\prime}O_{Oa,CN-4}{}''\square_{Oa,6-CN}O_{Oe,2}) + \frac{l+3-2CN}{4}(V_VO_{Oa,2}{}''O_{Oe,2})$
(c) Substitution for average vanadium polyhedron, where $2CN < (l + 6)$.
$(l + 7 - 2CN)\ (V_VO_{Oa,1.5}\square_{Oa,0.5}O_{Oe,2}) \rightarrow (M_V{}^{(5-l)\prime}O_{Oa,CN-4}{}^{(5.5-CN)(5-CN)\prime}\square_{Oa,6-CN}{}^{(5.5-CN)(CN-3)\cdot}O_{Oe,2}) + (l + 6 - 2CN)(V_VO_{Oa,2}{}^{0.5'}O_{Oe,2})$

Scheme 8 AV model, $4 \leqslant CN \leqslant 6$, no net change in vacancies.
(a) Substitution for octahedral vanadium, where $2CN = (7 + l)$.
$(V_VO_{Oa,2}O_{Oe,2}) \rightarrow (M_V{}^{(5-l)\prime}O_{Oa,CN-4}\square_{Oa,6-CN}{}^{\cdot\bullet}O_{Oe,2})$
(b) Substitution for tetrahedral vanadium, where $2CN = (3 + l)$.
$(V_V\square_{Oa,2}O_{Oe,2}) \rightarrow (M_V{}^{(5-l)\prime}O_{Oa,CN-4}{}''\square_{Oa,6-CN}O_{Oe,2})$
(c) Substitution for average vanadium polyhedron, where $2CN = (6 + l)$.
$(V_VO_{Oa,1.5}\square_{Oa,0.5}O_{Oe,2}) \rightarrow (M_V{}^{(5-l)\prime}O_{Oa,CN-4}{}^{(5.5-CN)(5-CN)\prime}\square_{Oa,6-CN}{}^{(5.5-CN)(CN-3)\cdot}O_{Oe,2})$

combinations of metal dopant charge and coordination number. The general forms of these schemes for metal dopants of charge *l*+ and *CN*s between four and six are given in Table 4.†

For dopant metal *CN*s between four and six the total vacancy concentration per V/M atom, $N_{\square}$, will be the sum of the intrinsic vacancies ($0.5 + \delta$) and the extrinsic vacancies caused by aliovalency of the metal dopant (eqn. (9)).

$$N_{\square} = 0.5 + \frac{(5-l)x}{2} + \delta \tag{9}$$

As can be seen in Table 4, for *CN*s lower than six some of the extrinsic vacancies/interstitials will be trapped on the metal dopant polyhedra and probably will not be involved in conduction. It is therefore useful to calculate the number of vacancies associated exclusively with vanadium polyhedra, $N_{\square V}$ by subtracting those trapped on the metal dopant polyhedra. The resulting number of oxygen vacancies per vanadium atom are given in eqns. (10) and (11) for EV and AV models respectively.

$$N_{\square V(EV)} = 0.5 + \frac{(5-l)x}{2} - \frac{(6-CN)x}{2} + \delta$$

$$\Rightarrow \quad N_{\square V(EV)} = 0.5 + \frac{(CN-1-l)x}{2} + \delta \tag{10}$$

$$N_{\square V(AV)} = 0.5 + \frac{(5-l)x}{2} - (5.5-CN)x + \delta$$

$$\Rightarrow \quad N_{\square V(AV)} = 0.5 + \frac{(2CN-6-l)x}{2} + \delta \tag{11}$$

For dopants with *CN*s greater than six the location of the additional oxide ion(s) required to make up the coordination polyhedron needs to be considered. Interstitial oxide ions may be located in a non-bridging position where they are exclusively associated with a single dopant polyhedron. Alternatively, they may be shared between dopant polyhedra. In the latter case this would necessitate clustering of dopant polyhedra. The general substitution schemes for metal dopants with coordination

Table 5 General schemes for substitution of V in BIMEVOXes by M^{l+} ions with preferred coordination number *CN* (where $CN > 6$)

Scheme 9 EV model, $CN > 6$, shared (bridging) interstitial oxygen.
(a) Substitution for vanadium octahedron.
$\frac{CN+1-l}{2}(V_V O_{Oa,2} O_{Oe,2}) \rightarrow (M_V^{(5-l)\prime} O_{Oa,2} O_{Oe,2} O_{is,(CN-6)/2}'') + \frac{CN-1-l}{2}(V_V O_{Oa,2} O_{Oe} \square_{Oe}^{\cdot\cdot})$
(b) Substitution for vanadium tetrahedron.
$(V_V O_{Oa,2} O_{Oe} \square_{Oe}) + \frac{CN+1-l}{2}(V_V O_{Oa,2} O_{Oe,2}) \rightarrow (M_V^{(5-l)\prime} O_{Oa,2} O_{Oe} O_{Oe}'' O_{is,(CN-6)/2}'') + \frac{CN+1-l}{2}(V_V O_{Oa,2} O_{Oe} \square_{Oe}^{\cdot\cdot})$
(c) Substitution for average vanadium polyhedron
$(CN + 1 - l)\,(V_V O_{Oa,2} O_{Oe,1.5} \square_{Oe,0.5}) \rightarrow (M_V^{(5-l)\prime} O_{Oa,2} O_{Oe,1.5} O_{Oe,0.5}'' O_{is,(CN-6)/2}'') + (CN - l)\,(V_V O_{Oa,2} O_{Oe} \square_{Oe}^{\cdot})$

Scheme 10 EV model, $CN > 6$, unshared (non-bridging) interstitial oxygen.
(a) Substitution for vanadium octahedron.
$\frac{2CN-5-l}{2}(V_V O_{Oa,2} O_{Oe,2}) \rightarrow (M_V^{(5-l)\prime} O_{Oa,2} O_{Oe,2} O_{iu,(CN-6)}'') + \frac{2CN-7-l}{2}(V_V O_{Oa,2} O_{Oe} \square_{Oe}^{\cdot\cdot})$
(b) Substitution for vanadium tetrahedron.
$(V_V O_{Oa,2} O_{Oe} \square_{Oe}) + \frac{2CN-5-l}{2}(V_V O_{Oa,2} O_{Oe,2}) \rightarrow (M_V^{(5-l)\prime} O_{Oa,2} O_{Oe} O_{Oe}'' O_{iu,(CN-6)}'') + \frac{2CN-5-l}{2}(V_V O_{Oa,2} O_{Oe} \square_{Oe}^{\cdot\cdot})$
(c) Substitution for average vanadium polyhedron
$(2CN - 5 - l)(V_V O_{Oa,2} O_{Oe,1.5} \square_{Oe,0.5}) \rightarrow (M_V^{(5-l)\prime} O_{Oa,2} O_{Oe,1.5} O_{Oe,0.5}'' O_{iu,(CN-6)}'') + (2CN - 6 - l)\,(V_V O_{Oa,2} O_{Oe} \square_{Oe}^{\cdot})$

Scheme 11 AV model, $CN > 6$, shared (bridging) interstitial oxygen.
(a) Substitution for octahedral vanadium
$\frac{CN+3-l}{4}(V_V O_{Oa,2} O_{Oe,2}) \rightarrow (M_V^{(5-l)\prime} O_{Oa,2} O_{Oe,2} O_{is,(CN-6)/2}'') + \frac{CN-1-l}{4}(V_V \square_{Oa,2}^{\cdot\cdot} O_{Oe,2})$
(b) Substitution for tetrahedral vanadium
$(V_V \square_{Oa,2} O_{Oe,2}) + \frac{CN+3-l}{4}(V_V O_{Oa,2} O_{Oe,2}) \rightarrow (M_V^{(5-l)\prime} O_{Oa,2}'' O_{Oe,2} O_{is,(CN-6)/2}'') + \frac{CN+3-l}{4}(V_V \square_{Oa,2}^{\cdot\cdot} O_{Oe,2})$
(c) Substitution for average vanadium polyhedron
$\frac{CN+3-l}{3}(V_V O_{Oa,1.5} \square_{Oa,0.5} O_{Oe,2}) \rightarrow (M_V^{(5-l)\prime} O_{Oa,2}^{0.5\prime} O_{Oe,2} O_{is,(CN-6)/2}'') + \frac{CN-l}{3}(V_V \square_{Oa,2}^{1.5\cdot} O_{Oe,2})$

Scheme 12 AV model, $CN > 6$, unshared (non-bridging) interstitial oxygen.
(a) Substitution for octahedral vanadium
$\frac{2CN-3-l}{4}(V_V O_{Oa,2} O_{Oe,2}) \rightarrow (M_V^{(5-l)\prime} O_{Oa,2} O_{Oe,2} O_{iu,(CN-6)}'') + \frac{2CN-7-l}{4}(V_V \square_{Oa,2}^{\cdot\cdot} O_{Oe,2})$
(b) Substitution for tetrahedral vanadium
$(V_V \square_{Oa,2} O_{Oe,2}) + \frac{2CN-3-l}{4}(V_V O_{Oa,2} O_{Oe,2}) \rightarrow (M_V^{(5-l)\prime} O_{Oa,2}'' O_{Oe,2} O_{iu,(CN-6)}'') + \frac{2CN-3-l}{4}(V_V \square_{Oa,2}^{\cdot\cdot} O_{Oe,2})$
(c) Substitution for average vanadium polyhedron
$\frac{2CN-3-l}{3}(V_V O_{Oa,1.5} \square_{Oa,0.5} O_{Oe,2}) \rightarrow (M_V^{(5-l)\prime} O_{Oa,2}^{0.5\prime} O_{Oe,2} O_{iu,(CN-6)}'') + \frac{2CN-6-l}{3}(V_V \square_{Oa,2}^{1.5\cdot} O_{Oe,2})$

numbers greater than six are given in Table 5. In these cases further vacancies are created and since all vacancies must be associated exclusively with vanadium polyhedra, eqn. (9) is modified as in eqns. (12) and (13).

$$N_{\square} = N_{\square V} = 0.5 + \frac{(5-l)x}{2} + \frac{(CN-6)x}{2} + \delta \qquad (12)$$

(for shared interstitials)

$$N_{\square} = N_{\square V} = 0.5 + \frac{(5-l)x}{2} + (CN-6)x + \delta \qquad (13)$$

(for unshared interstitials)

5 Solid solution limits

Assuming a minimum coordination number of four for vanadium, in both the AV and EV models, for a solid solution that involves vacancy creation, the theoretical maximum vacancy concentration occurs either when all V are substituted or all V are four-coordinate. The dopant concentration at which this occurs represents the theoretical solid solution limit. Therefore, for a system that involves a four-coordinate dopant, the maximum vacancy concentration in the AV model is two per V/M atom, while in the EV model it is only one per V/M atom. Conversely, in solid solution systems where vacancies are consumed, the minimum vacancy concentration represents the theoretical limiting case for solid solutions and occurs either on full substitution of V or when all remaining V are six-coordinate.

From the substitutions for average vanadium polyhedra in Tables 4 and 5 the solid solution limits are immediately apparent. For example, in a trivalent substituted system where the metal adopts a six-coordinate environment, for every average vanadium polyhedron substituted, electroneutrality requires, that in the EV model, a further three are converted to vanadium tetrahedra. Therefore, only one in four vanadium atoms can be substituted and the theoretical solid solution limit is 0.25. For the same system the AV model predicts that one in two vanadium atoms can be substituted giving a solid solution limit of 0.5. Clearly if the observed limit is higher than 0.25, some or all of the vacancies are located in apical positions.

Eqns. (14)–(17) show how the theoretical solid solution limits can be calculated for the general BIMEVOX systems outlined in Table 4.

EV model ($4 \leq CN \leq 6$)

$$x_{max} = \frac{1-2\delta}{CN+1-l} \qquad (\text{for } CN \geq l) \qquad (14)$$

$$x_{max} = \frac{1+2\delta}{l-CN+1} \qquad (\text{for } CN \leq l) \qquad (15)$$

AV model ($4 \leq CN \leq 6$)

$$x_{max} = \frac{3-2\delta}{2CN-3-l} \qquad (\text{For } 2CN \geq l+6) \qquad (16)$$

$$x_{max} = \frac{1+2\delta}{l+7-2CN} \qquad (\text{For } 2CN \leq l+6) \qquad (17)$$

For higher *CN*s, in the EV model, if the additional oxide ions required for the metal polyhedron are shared with other polyhedra then eqn. (14) holds (*CN* is always greater than or equal to *l* in these cases). For unshared interstitials eqn. (18) applies.

EV model ($CN > 6$, unshared interstitials)

$$x_{max} = \frac{1-2\delta}{2CN-5-l} \qquad (18)$$

Similarly in the AV model eqn. (16) holds in the case of unshared interstitials. For shared interstitials eqn. (19) is required.

Table 6 Theoretical solid solution limits (x_{max}) in BIMEVOXes, where dopant metal ion, M^{l+}, adopts coordination number, CN[a]

(a) EV model all interstitials/vacancies bridging

l	$CN = 4$	$CN = 5$	$CN = 6$	$CN = 7$	$CN = 8$
+1	0.250	0.200	0.167	0.143	0.125
+2	0.333	0.250	0.200	0.167	0.143
+3	0.500	0.333	0.250	0.200	0.167
+4	1.000	0.500	0.333	0.250	0.200
+5	0.500	1.000	0.500	0.333	0.250
+6	0.333	0.500	1.000	0.500	0.333

(b) EV model $CN > 6$ non-bridging additional interstitials

l	$CN = 7$	$CN = 8$
+1	0.125	0.100
+2	0.143	0.111
+3	0.167	0.125
+4	0.200	0.143
+5	0.250	0.167
+6	0.333	0.200

(c) AV model

l	$CN = 4$	$CN = 5$	$CN = 6$	$CN = 7$	$CN = 8$
+1	0.750	0.500	0.375	0.300	0.250
+2	1.000	0.600	0.429	0.333	0.273
+3	0.500	0.750	0.500	0.375	0.300
+4	0.333	1.000	0.600	0.429	0.333
+5	0.250	0.500	0.750	0.500	0.375
+6	0.200	0.333	1.000	0.600	0.429

(d) AV model $CN > 6$ bridging additional interstitials

l	$CN = 7$	$CN = 8$
+1	0.333	0.300
+2	0.375	0.333
+3	0.429	0.375
+4	0.500	0.429
+5	0.600	0.500
+6	0.750	0.600

[a]Calculated using the program SSLCN, a listing of which is included as supplementary information.

AV model ($CN > 6$, shared interstitials)

$$x_{max} = \frac{3-2\delta}{CN+3-l} \quad (19)$$

Assuming that the value of δ is negligible then eqns. (14)–(19) allow for the calculation of theoretical solid solution limits for all combinations of CN and l for the two vacancy models. These are summarised in Table 6. The theoretical limits in Table 6 do not take into account the thermodynamic stability of the resultant BIMEVOX phases, which can cause a lowering of the observed limit. Nevertheless, they do provide a useful way of rationalising observed differences in solid solution limits and can indicate the preferred substitution mechanism in a particular system.

Observed solid solution limits for a number of BIMEVOX systems are given in Table 7. In many cases only selected BIMEVOX compositions have been synthesised and the exact solid solution limits are somewhat ambiguous. This can to a limited extent explain the discrepancies between studies by different groups. It is however evident that there is significant variation in the observed limits not only between BIMEVOXes with dopants of different charge, but also between those of the same charge. In the case of the best studied BIMEVOXes, the divalent substituted systems, the EV model predicts theoretical

Table 7 Observed γ'-phase stabilisation onset compositions and solid solution limits in selected BIMEVOX systems of general formula $Bi_2M'^{l+}{}_xV_{1-x}O_{5.5-(5-l)x/2-\delta}$

M'^{l+}	γ'-Phase onset (x)	Solid solution limit (x)	References
M^{2+}			
Mg^{2+}	0.075	0.15	7
	0.10–0.13	0.30	43
Co^{2+}	0.10	0.19–0.22	38
	0.075	0.25	2, 34
		0.33	56
	0.10	0.225	57
	0.075	0.175	58
Ni^{2+}	0.10		7
	0.10	0.20	39
Cu^{2+}	0.075	0.125	7
	0.07	0.12	31
		0.135	56
Zn^{2+}	0.10	0.25	58
	0.125	0.25	2
	0.10	0.25	50
	0.125	0.25	59
	0.13	0.25	58
M^{3+}			
Al^{3+}	0.10	0.30	60
Cr^{3+}	0.10	0.35	58
Mn^{3+}	0.075	0.25	61
	0.10	0.25	62
Fe^{3+}	0.15	0.25	63
M^{4+}			
Ti^{4+}	0.10	0.20	7
	0.10	0.15	62
V^{4+}		1.00	13
Zr^{4+}	0.10	0.15	7
	0.10	0.15	62
	0.16	0.22	46
M^{5+}			
Sb^{5+}	0.15	0.50	51
Nb^{5+}	0.15	0.30	51
	0.10	0.50	7
Ta^{5+}	0.10	0.25	7

solid solution limits of $x_{max} = 0.33$, 0.25 and 0.20 for metal dopant coordination numbers of 4, 5 and 6 respectively. The analogous limits predicted using the AV model are $x_{max} = 1.00$, 0.60 and 0.43 respectively. The observed limits for the Ni^{2+}, Co^{2+} and Zn^{2+} substituted systems are all close to $x = 0.20$, *i.e.* close to the predicted limit for octahedral metal dopants in the EV model. Neutron diffraction studies on the Ni^{2+} substituted system confirms the exclusivity of equatorial vacancies for the $x = 0.10$ composition,[39] while in the Co doped system this was also confirmed for the $x = 0.20$ composition.[38] These results combined with the observed solid solution limits appear to indicate a preference for these dopants to adopt octahedral coordination in the vanadate layer with equatorial vacancies localised on vanadium tetrahedra. In contrast in the Mg^{2+} substituted system the BIMEVOX structure is maintained up to $x = 0.30$,[43] however at high compositions, around $x = 0.30$, a new orthorhombic phase related to the α and β polymorphs is observed. Neutron diffraction also confirms the exclusivity of the equatorial vacancies in this system for the $x = 0.10$ composition.[15] Therefore if we assume that only equatorial vacancies are present throughout the composition range, the Mg coordination must be tetrahedral.

For tetravalent substituted systems full substitution is predicted for tetrahedrally coordinated dopants. Indeed we have recently confirmed that the BIMEVOX structure is

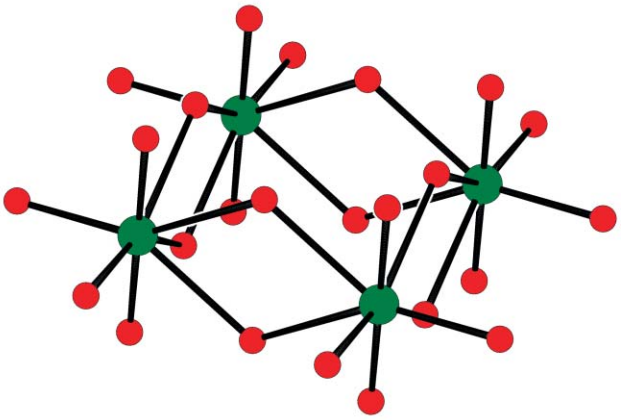

Fig. 8 Proposed clustering of Zr polyhedra in BIZRVOX. Oxygen and zirconium atoms are represented by red and green spheres respectively.

certainly maintained up to $x = 0.50$ in BISIVOX, $BiSi_xV_{1-x}O_{5.5-x/2-\delta}$,[44] and the structure of the end member, Bi_2SiO_5,[45] shows a close structural relationship to the BIMEVOXes. In a recent study on the BIZRVOX system, $BiZr_xV_{1-x}O_{5.5-x/2-\delta}$,[46] a solid solution limit of $x = 0.20$ was observed suggesting eight coordinate Zr as seen in cubic zirconia. The sharing of the additional interstitials would necessitate a clustering of four Zr polyhedra in order to achieve the required coordination number (Fig. 8).

For tetravalent substituted systems that show a preferential dopant coordination number of six, theoretical solid solution limits of $x = 0.33$ and 0.60 are predicted by the EV and AV models respectively. If we consider V^{4+} to be a dopant then the compound $Bi_4V_2O_{10.66}$ represents the solid solution limit in the EV model. Indeed in this structure a 2 : 1 ratio of tetrahedra to octahedra is observed.[11] Interestingly, under strongly reducing conditions it is possible to synthesise the fully reduced system $Bi_4V_2O_{10}$.[13] In this case the structure has been shown to contain V in a distorted square pyramidal coordination, which can be thought of as a defect octahedron with an apical vacancy and therefore corresponds exactly to the predicted end member for a tetravalent, five coordinate dopant in the AV model.

The neutron diffraction studies on the BIMEVOXes discussed above have revealed that under standard synthetic conditions vacancies appear to be concentrated in the bridging equatorial positions, which suggests that the EV model predominates.[15,38,39] However, there is also significant disorder in the non-bridging apical positions and the possibility of some vacancies being located on these sites cannot be entirely discounted. Indeed recent evidence suggests that in the monoclinic α-phase of $Bi_4V_2O_{11-\delta}$ there are apical as well as equatorial vacancies.[30] The EV model is not exclusive and it is clear that under certain synthetic conditions the AV model may be favoured as in $Bi_4V_2O_{10}$.[13] It is also possible that in certain systems both mechanisms operate in which case a solid solution limit between the two limiting models may be obtained. The degree of V reduction (δ) may also be significant in lowering the observed solid solution limit. As δ increases, the fraction of vanadium tetrahedra increases and hence the solid solution limit will be lowered in the case of vacancy creating systems or raised in the case of vacancy consuming systems. Thus the observed solid solution limit is predicted to vary with synthesis conditions and this may explain some of the discrepancies between the values reported by various authors.

6 Electrical conduction

The main interest in BIMEVOXes stems from their electrical conductivity performances, which are exceptional. Measurement of transport numbers indicate that conductivity is almost

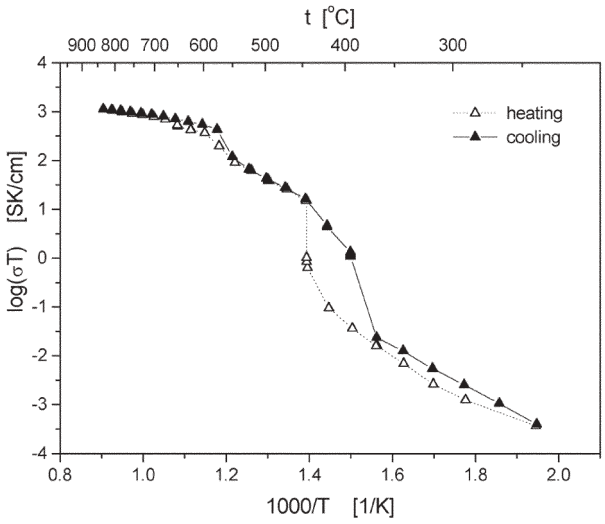

Fig. 9 Arrhenius plot of total conductivity for $Bi_4V_2O_{11-\delta}$.

exclusively ionic.[9] Most studies on electrical behaviour have been carried out on highly dense ceramics with densities approaching theoretical values. In the Arrhenius plot of total conductivity for the parent material three regions with different activation energies are observed, which are correlated with the stability ranges of the three principal phases α, β and γ (Fig. 9). Significant thermal hysteresis is observed at the α↔β transition. Single crystal studies have revealed the anisotropic nature of conductivity, with conductivity parallel to the *a–b* plane, $\sigma_{\parallel}$, nearly two orders of magnitude greater than conductivity perpendicular to the plane, $\sigma_{\perp}$.[2,47] This confirms that the principal contribution to ionic conductivity is intra-layer.

On substitution of V by metal cations, high temperature conductivity, as characterised by the conductivity at 600 °C, σ_{600}, generally decreases with a corresponding increase in the high temperature activation energy, ΔE_{HT}.[2,35,43,48–50] In the Zr substituted system, BIZRVOX, this decrease in σ_{600} shows an exponential decay (Fig 10).[46] In some cases, however, higher conductivities than in the parent compound, $Bi_4V_2O_{11-\delta}$, are observed for example in the isovalent substituted systems, $Bi_2Sb_xV_{1-x}O_{5.5-\delta}$ and $Bi_2Nb_xV_{1-x}O_{5.5-\delta}$.[51] The low temperature conductivities, as characterised by the conductivity at 300 °C, σ_{300}, generally possess higher values than that for the parent material and usually show a maximum at compositions close to the onset of γ′-phase stabilisation. The variation in σ_{300} with composition in BIMGVOX is shown in Fig. 11[43] and clearly shows a maximum at $x = 0.13$, which is coincident with the lower composition limit for room temperature stabilisation

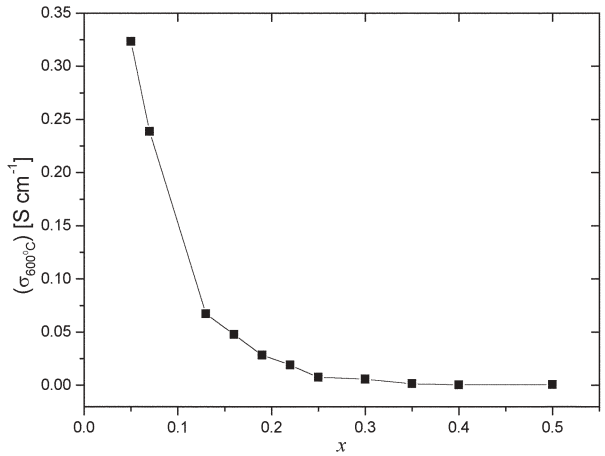

Fig. 10 Variation of σ_{600} with composition in BIZRVOX, $Bi_2Zr_xV_{1-x}O_{5.5-x/2-\delta}$.

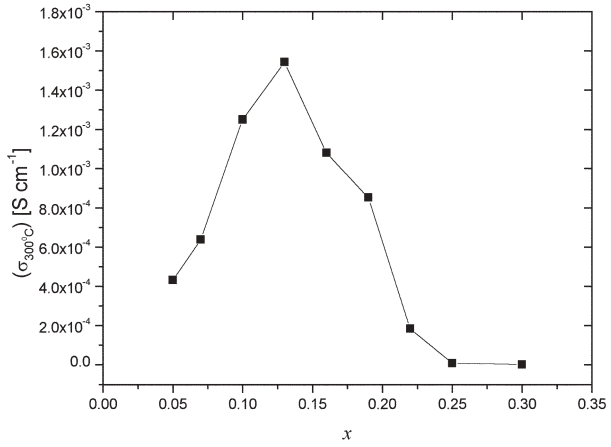

Fig. 11 Variation of σ_{300} with composition in BIMGVOX, $Bi_2Mg_xV_{1-x}O_{5.5-3x/2-\delta}$.

of the γ′-phase. Similar trends are seen in the other BIMEVOXes.[35,49,50]

The variation in activation energies between different dopant ions reflects the strength of the interaction between the dopant ions and the oxide ion vacancies. Activation energy generally increases with increasing charge on the dopant ion as this interaction gets stronger.

The main features of the Arrhenius plots of conductivity for the BIMEVOXes vary with composition. For low values of x, where the orthorhombic phases α or β are stable at room temperature, the Arrhenius plots reflect the various phase transitions. Fig. 12 shows the Arrhenius plot for BIZNVOX for the $x = 0.05$ composition, which is typical. On heating a gradual change is seen corresponding to the α→γ transition. However, on cooling sharper changes are observed associated with γ→β and β→α transitions. This form of thermal hysteresis is typical of the low x value composition BIMEVOXes. It is interesting to note that in the parent material, although thermal hysteresis is seen, the β phase is observed on heating as well as cooling. Clearly the addition of a dopant metal slows the kinetics of the α→β transition.

At higher values of x where the γ′-phase is stabilised at room temperature, two distinct regions are evident in the Arrhenius plots. A typical example is the Arrhenius plot for BINIVOX at the $x = 0.14$ composition, Fig. 3. The Arrhenius plot for this composition is fully reproducible with no thermal hysteresis. The two linear regions reflect the existence of two closely related phases, γ′ at low temperatures, with the higher activation

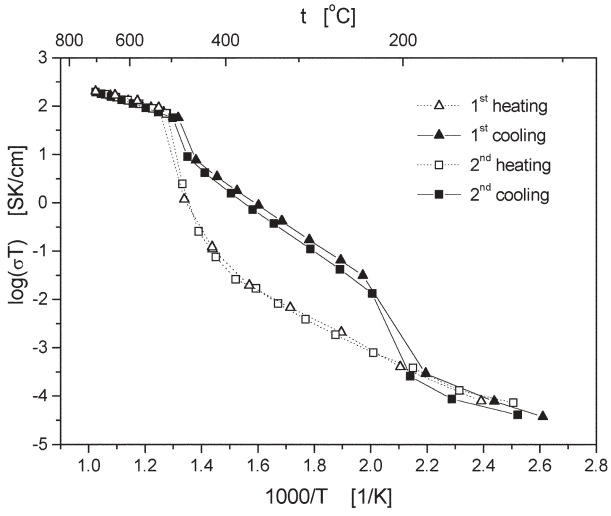

Fig. 12 Arrhenius plot of total conductivity for BIZNVOX.05, $Bi_2Zn_{0.05}V_{0.95}O_{5.425-\delta}$.

energy and γ at temperatures above *ca.* 450 °C with a lower activation energy. The higher activation energy of the γ′-phase is related to the ordering of the oxide ion vacancies that occurs in this incommensurately modulated phase. Therefore the γ′ activation energy has contributions not only from vacancy migration, but also from defect trapping effects in the superlattice, whereas in the γ-phase, the latter contribution is absent.

7 Model for conduction mechanism in BIMEVOXes

It has been established from measurements on BIMEVOX single crystals that oxide ion conduction is essentially two dimensional, with $\sigma_\perp < \sigma_\parallel$.[2,47] Therefore conduction must involve hopping of vacancies/oxide ions, parallel to the layer planes. As discussed above, evidence from neutron diffraction studies and observed solid solution limits strongly suggests that the EV model predominates in the BIMEVOXes. In order for conduction to occur in the vanadate layer, oxide ions and vacancies must exchange positions and therefore in the dynamic system the V octahedra and tetrahedra are likely to be in a state of flux. There are a number of ways in which this could be achieved, but the absence of vacancies in the apical positions suggests that only the equatorial O(3) ions are involved. It is also likely that oxygen ions or vacancies associated with the dopant polyhedra are trapped on those polyhedra and are unlikely to be directly involved in conduction. A possible basic mechanism is summarised in Scheme 13. The intermediate situation involves the formation of five coordinate vanadium polyhedra.

Scheme 13 $(V_VO_{Oa,2}O_{Oe,2}) + (V_VO_{Oa,2}O_{Oe}\square_{Oe}) \rightarrow (V_VO_{Oa,2}O_{Oe,1.5}\square_{Oe,0.5}^{\bullet\bullet}) + (V_VO_{Oa,2}O_{Oe}O_{Oe,0.5}''\square_{Oe,0.5}) \rightarrow (V_VO_{Oa,2}O_{Oe}\square_{Oe}^{\bullet\bullet}) + (V_VO_{Oa,2}O_{Oe}O_{Oe}'')$

For oxide ion diffusion to occur a suitable pathway must be available. The most likely route is through the interstitial vacant site located in the equatorial vanadate plane between four vanadium polyhedra. This site, as indicated earlier, is faced by two Bi $6s^2$ lone pair orbitals arranged in a linear "coordination". The polarizibility of the lone pair orbitals in heavier main group subvalent metals is well known, so despite the electrostatic repulsion endured by transient oxide ions occupying this site, this route represents a favourable one as it avoids close proximity to the V atoms. Nevertheless, it is unlikely that the residence time in this site is long. Indeed no significant scattering from this site is noted in the neutron diffraction studies.[15,37–39]

To illustrate the possible mechanism of ionic conductivity it is helpful to take as a starting point a typical BIMEVOX composition with a ratio of 3 : 1 tetrahedra to octahedra.[52] In this case the proposed mechanism involves four neighbouring V polyhedra. The first step in the mechanism involves the movement of an oxide ion from a bridging equatorial site *via* the interstitial site to an equatorial vacancy on a neighbouring V polyhedron (Fig. 13a). In the case illustrated in Fig. 13 the oxide ion that moves is originally shared between a vanadium octahedron and a vanadium tetrahedron. This first step yields an intermediate situation of two tetrahedra and two five coordinate V polyhedra (Fig. 13b). The second step involves movement of a second oxide ion from one of the five-coordinate vanadium polyhedra to the other, resulting in the starting situation of one octahedron and three tetrahedra (Fig. 13c). Overall the process results in the effective mobility of vanadium octahedra and tetrahedra within the vanadate layer. Similar mechanisms can be devised for different ratios of vanadium polyhedra, but in each case the overall result is as shown in Scheme 13. The model presented is somewhat simplified since the rearrangement of tetrahedra in both

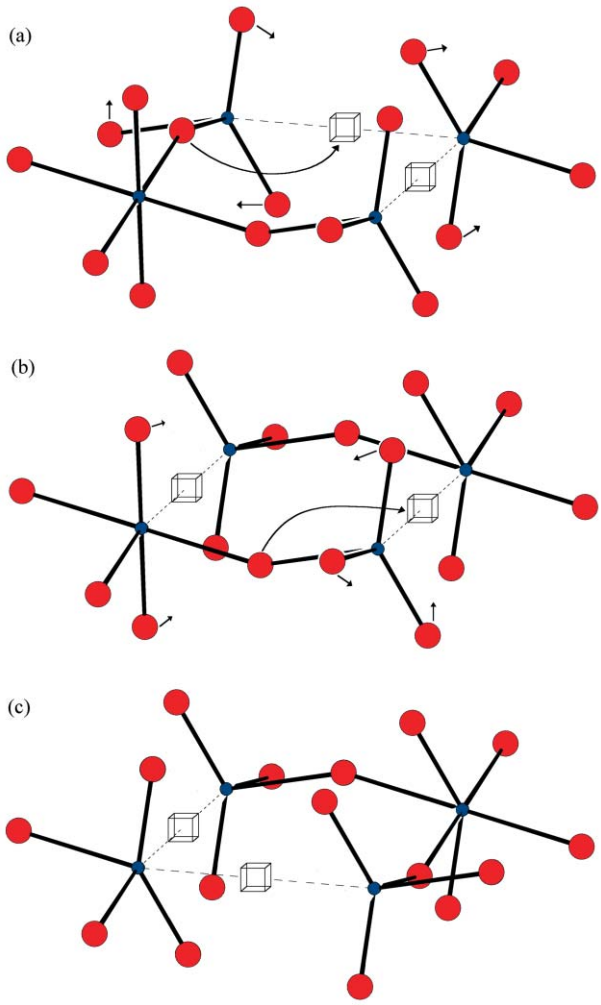

Fig. 13 Model of conduction mechanism in BIMEVOXes, showing (a) starting, (b) intermediate and (c) final situations.

steps can involve creation of further neighbouring equatorial vacancies as oxide ions switch from corner sharing to terminal coordination.

8 Conclusions

The BIMEVOXes are a unique family of compounds in which V can be substituted by a variety of cations almost irrespective of the radius of the dopant cation. We have shown that from an understanding of the defect structure of BIMEVOXes general models for substitutional solid solution formation can be derived and from these theoretical solid solution limits can be obtained. It is clear that the preferred coordination number of the metal dopant as well as its cationic charge are important in determining the observed solid solution limit.

A knowledge of the defect structure also allows for the development of a model for the conduction mechanism, which involves movement of equatorial oxide ions/vacancies between octahedral and tetrahedral vanadium polyhedra *via* a vacant interstitial site located at the central point between four vanadium polyhedra and linearly "coordinated" to two Bi $6s^2$ lone pairs of electrons. This type of interstitial site is similar to that seen in $Bi_2Al_4O_9$[53] and is one of two types of interstitial site common in Bi_2O_3 based electrolytes, the other being tetrahedrally "coordinated" as in δ-Bi_2O_3[54] and β_{III}-$Bi_{1.85}Zr_{0.15}O_{3.075}$.[55] Key to high conductivity are the relative concentrations of equatorial oxide ions and vacancies located on the vanadium polyhedra, *i.e.* the ratio of vanadium octahedra to tetrahedra. In the parent compound ($x = 0.0$) the value of X_{tet} is calculated as 0.5 in the EV model and hence there are equal numbers of octahedra and tetrahedra. As the dopant level increases the value of X_{tet} increases and consequently the number of available oxide ions in equatorial positions on V octahedra decreases. This correlates with the lowering of high temperature (above *ca.* 500 °C) conductivity with respect to the parent γ-$Bi_4V_2O_{11-\delta}$. The presence of dopant ions with a preferred coordination number effectively traps defects and therefore also lowers conductivity.

The unrivalled low temperature conductivity of the BIMEVOXes is attributable to a unique combination of structural features: (i) the variable coordination environment of V with four, five and six coordinate polyhedra common in oxide systems; (ii) the presence of an available interstitial conduction site surrounded by two polarizable Bi $6s^2$ lone pairs and (iii) high concentrations of mobile species.

Although we now have a good understanding of the defect chemistry of the BIMEVOXes, the composition dependency of γ′-phase stabilisation is still not well understood. The reasons for the thermodynamic stability of the γ′-phase over the orthorhombic phases α and β at particular compositions remain unclear. It is however, evident that experimental conditions have an important role as there are large discrepancies between workers as to the stability ranges of the γ′-phases of particular BIMEVOXes. Similarly it is unclear as to whether the γ–γ′ transition is due to metastability of the γ-phase with respect to the γ′ phase or small compositional variation due to reduction/oxidation of vanadium. Indeed recent evidence suggests that the latter may be the case.[15] Nevertheless, as was previously suggested by Goodenough *et al.*,[7] the dopant–vacancy interaction appears critical in facilitating the order–disorder transition.

The EV and AV models presented here only take into account substitution for V. While it is certainly likely that some BIMEVOX systems show substitution for Bi, for example BiPBVOX, there has been some argument as to whether other BIMEVOXes show substitution of Bi such as the lanthanide doped systems. The models presented here require some modification to account for substitution for Bi, however the principles used are the same. The complication arises when both V and Bi are considered to be substituted in the same system.

Acknowledgement

We gratefully acknowledge The Royal Society of Chemistry for a Journals Grant for International Authors.

References

1 See for example, B. C. H. Steele, in *High Conductivity Solid Ionic Conductors. Recent Trends and Applications*, ed. T. Takahashi, World Scientific, Singapore, 1989; N. Q. Minh, *J. Am. Ceram. Soc.*, 1993, **76**, 563; J. Kilner, S. Benson, J. Lane and D. Waller, *Chem. Ind.*, 1997, 907.
2 G. Mairesse, in *Fast Ion Transport in Solids*, eds. B. Scrosati, A. Magistris, C. M. Mari, G. Mariotto, Kluwer Academic Publishers, Dordrecht, 1993, p. 271.
3 J. C. Boivin and G. Mairesse, *Chem. Mater.*, 1998, **10**, 2870.
4 P. Shuk, H. D. Wiemhöfer, U. Guth, W. Göpel and M. Greenblatt, *Solid State Ionics*, 1996, **89**, 179.
5 N. M. Sammes, G. A. Tompsett, H. Näfe and F. Aldinger, *J. Eur. Ceram. Soc.*, 1999, **19**, 1801.
6 A. M. Azad, S. Larose and S. A. Akbar, *J. Mater. Sci.*, 1994, **29**, 4135.
7 J. B. Goodenough, A. Manthiram, M. Paranthaman and Y. S. Zhen, *Mater. Sci. Eng., Sect. B*, 1992, **12**, 357.
8 F. Abraham, M. F. Debreuille-Gresse, G. Mairesse and G. Nowogrocki, *Solid State Ionics*, 1988, **28–30**, 529.
9 F. Abraham, J. C. Boivin, G. Mairesse and G. Nowogrocki, *Solid State Ionics*, 1990, **40/41**, 934.
10 C. K. Lee, D. C. Sinclair and A. R. West, *Solid State Ionics*, 1993, **62**, 193.
11 M. Huve, M. R. N. Vannier, G. Nowogrocki, G. Mairesse and G. J. VanTendeloo, *Mater Chem.*, 1996, **6**, 1339.

12 I. Abrahams, A. J. Bush, F. Krok, G. E. Hawkes, K. D. Sales, P. Thornton and W. Bogusz, *J. Mater. Chem.*, 1998, **8**, 1213.
13 J. Galy, R. Enjalbert, P. Millan and A. Castro, *C. R. Acad. Sci. Paris, Ser. II*, 1993, **317**, 43.
14 A. Castro, P. Millán, J. Ricote and L. Pardo, *J. Mater. Chem.*, 2000, **10**, 767.
15 I. Abrahams, F. Krok, M. Malys and A. J. Bush, *J. Mater. Sci.*, 2001, **36**, 1099.
16 S. Sorokina, S. Enjalbert, R. Baules, P. Castro and A. Galy, *J. Solid State Chem.*, 1999, **144**, 379.
17 P. Millán, J. M. Rojo and A. Castro, *Mater. Res. Bull.*, 2000, **35**, 835.
18 A. K. Bhattacharya, K. K. Mallick and P. A. Thomas, *Solid State Commun.*, 1994, **91**, 357.
19 K. Shantha and K. B. R. Varma, *J. Mater. Res.*, 1999, **14**, 4651.
20 K. Shantha, G. N. Subbanna and K. B. R. Varma, *J. Solid State Chem.*, 1999, **142**, 41.
21 J. W. Pell, K. M. Delak and H.-C. zur Loye, *Chem. Mater.*, 1998, **10**, 1764.
22 D. Barreca, L. E. Depero, V. Di Noto, G. A. Rizzi, L. Sangaletti and E. Tondello, *Chem. Mater.*, 1999, **11**, 255.
23 J. W. Pell, R. C. Y. Auyeung, D. B. Chrisey and H.-C. zur Loye, *Thin Solid Films*, 1997, **300**, 154.
24 M. Touboul, J. Lokaj, L. Tessier, V. Kettman and V. Vrabel, *Acta Crystallogr., Sect. C*, 1992, **48**, 1176.
25 P. Kurek, P. Pontgratz and M. W. Breiter, *Solid State Ionics*, 1998, **113–115**, 615.
26 P. I. Paulin, M. R. Morelli and S. C. Maestrelli, *Mater. Res. Innovations*, 2000, **3**, 292.
27 M. H. Paydar, A. M. Hadian, K. Shiamnoe and N. Yamazoe, *J. Eur. Ceram. Soc.*, 2001, **21**, 1825.
28 B. Vaidhyanathan, K. Balaji and K. J. Rao, *Chem. Mater.*, 1998, **10**, 3400.
29 O. Joubert, A. Jouanneaux and M. Ganne, *Mater. Res. Bull.*, 1994, **29**, 175.
30 R. N. Vannier, presented at *6th International Symposium on Systems with Fast Ionic Transport*, 9–12 May, 2001, Cracow, Poland.
31 E. Pernot, M. Anne, M. Bacmann, P. Strobel, J. Fouletier, R. N. Vannier, G. Mairesse, F. Abraham and G. Nowogrocki, *Solid State Ionics*, 1994, **70/71**, 259.
32 J. Zemann, *Beitr. Mineral. Petrogr.*, 1956, **5**, 139; A. F. van den Elzen and G. D. Rieck, *Acta Crystallogr., Sect. B*, 1973, **29**, 2436; F. Pertlik and J. Zemann, *Fortschr. Mineral., Beih.*, 1982, **60**, 162; R. G. Teller., J. F. Brazdil, R. K. Grasselli and J. D. Jorgensen, *Acta Crystallogr., Sect. C*, 1984, **40**, 2001; F. R. Theobald, A. Laarif and A. W. Hewat, *Ferroelectrics*, 1984, **56**, 219; D. J. Buttrey, D. A. Jefferson and J. M. Thomas, *Philos. Mag. A*, 1986, **53**, 897.
33 K. Shanta and K. B. R. Varma, *Solid State Ionics*, 1997, **99**, 225.
34 S. Lazure, R. N. Vannier, G. Nowogrocki, G. Mairesse, C. Muller, M. Anne and P. Strobel, *J. Mater. Chem.*, 1995, **5**, 1395.
35 F. Krok, I. Abrahams, D. G. Bangobango, W. Bogusz and J. A. G. Nelstrop, *Solid State Ionics*, 1996, **86–88**, 261.
36 C. Muller, M. Anne and M. Bacmann, *Solid State Ionics*, 1998, **111**, 27.
37 C. Muller, M. Anne, M. Bacmann and M. Bonnet, *J. Solid State Chem.*, 1998, **141**, 241.
38 I. Abrahams, F. Krok and J. A. G. Nelstrop, *Solid State Ionics*, 1996, **90**, 57.
39 I. Abrahams, J. A. G. Nelstrop, F. Krok and W. Bogusz, *Solid State Ionics*, 1998, **110**, 95.
40 F. Krok, M. Malys, J. R. Dygas, W. Bogusz and I. Abrahams, *Mol. Phys. Rep.*, 2000, **27**, 46.
41 *IUPAC Nomenclature of Inorganic Chemistry Recommendations 1990*, ed G.J. Leigh, Blackwell Scientific Publications, Oxford, 1991, p. 72; R. J. D. Tilley, *Defect Crystal Chemistry and its Applications*, Blackie and Son Ltd., Glasgow, 1987, p. 90.
42 *ICSD-Inorganic Crystal Structure Data Release 9301*, University of Bonn and Gmelin Insitute, Bonn, 1993.
43 F. Krok, I. Abrahams, M. Malys, W. Bogusz, J. R. Dygas, J. A. G. Nelstrop and A. J. Bush, *Solid State Ionics*, 2000, **136/137**, 119.
44 F. Krok, I. Abrahams, A. Kozanecka and S. C. M Chan, unpublished results.
45 J. Ketterer and V. Kraemer, *Neues Jahrb. Mineral., Monatsh.*, 1986, **13**, 1986.
46 F. Krok, I. Abrahams, W. Wrobel, S. C. M. Chan, M. Malys, W. Bogusz and J. R. Dygas, *Solid State Ionics*, in press.
47 S.-K. Kim and M. Miyayama, *Solid State Ionics*, 1997, **104**, 295.
48 L. Qui, Y. L. Yang and A. J. Jacobson, *J. Mater. Chem.*, 1997, **7**, 249.
49 F. Krok, I. Abrahams, D. Bangobango, W. Bogusz and J. A. G. Nelstrop, *Solid State Ionics*, 1998, **111**, 37.
50 F. Krok, I. Abrahams, A. Zadrozna, M. Malys, W. Bogusz, J. A. G. Nelstrop and A. J. Bush, *Solid State Ionics*, 1999, **119**, 139.
51 O. Joubert, A. Jouanneaux, M. Ganne, R. N. Vannier and G. Mairesse, *Solid State Ionics*, 1994, **73**, 309.
52 I. Abrahams and F. Krok, *Solid State Ionics*, in press.
53 I. Abrahams, A. J. Bush, G. E. Hawkes and T. Nunes, *J. Solid State Chem.*, 1999, **147**, 631.
54 G. Gattow and H. Schroeder, *Z. Anorg. Allg. Chem.*, 1962, **176**, 318; F. Hund, *Z. Anorg. Allg. Chem.*, 1964, **248**, 333; H. A. Harwig, *Z. Anorg. Allg. Chem.*, 1978, **151**, 444; P. D. Battle, C. R. A. Catlow, J. Drennan and A. D. Murray, *J. Phys. C.*, 1983, **16**, L561.
55 I. Abrahams, A. J. Bush, S. C. M. Chan, F. Krok and W. Wrobel, *J. Mater. Chem.*, 2001, **11**, 1715.
56 C. K. Lee, G. S. Lim and A. R. West, *J. Mater. Chem.*, 1994, **4**, 1441.
57 R. Essalim, B. Tanouti, J. P. Bonnet and J. M. Reau, *Mater. Lett.*, 1992, **13**, 382.
58 S. Lazure, Ch. Vernochet, R. N. Vannier, G. Nowogrocki and G. Mairesse, *Solid State Ionics*, 1996, **90**, 117.
59 C. Vernochet, R. N. Vannier, M. Huve, C. Pirovano, G. Nowogrocki, G. Mairesse and S. Van Tendeloo, *J. Mater. Chem.*, 2000, **10**, 2811.
60 C. K. Lee, B. H. Bay and A. R. West, *J. Mater. Chem.*, 1996, **6**, 331.
61 M. Alga, M. Wahbi, A. Ammar, B. Tanouti, J. C. Grenier and J. M. Reau, *J. Alloys Compd.*, 1997, **256**, 234.
62 J. Yan and M. Greenblatt, *Solid State Ionics*, 1995, **81**, 255.
63 O. Joubert, M. Ganne, R. N. Vannier and G. Mairesse, *Solid State Ionics*, 1996, **83**, 199.